

Design of a spaceborne astrometric survey instrument

Robert D. Reasenberg and James D. Phillips*

Smithsonian Astrophysical Observatory
Harvard-Smithsonian Center for Astrophysics
60 Garden Street, Cambridge, MA 02138

ABSTRACT

We have investigated the design of a small astrometric and photometric survey instrument in the Hipparcos tradition. Such a mission will support a rich and diverse ensemble of scientific investigations. The design objectives, which have been met in this study, are to be able to measure 10^7 stars over the full sky, with an accuracy of 0.05 mas for mag < 9 and 20 mas for mag 15. A scanning survey instrument that uses CCD detectors is able to measure many stars simultaneously. As compared to a pointed astrometric instrument of comparable size, the survey instrument generally has much higher measurement throughput (sum over targets of the inverse variance), but on average, less scientific interest per target. An instrument for astrometry, unlike those for imaging, can be compact and yet scientifically productive.

We report on a study of a Fast Astrometric Mapping Explorer (FAME-98) and an examination of standard approaches for scanning astrometric missions. We find some of these standard approaches wanting. We have concluded that a scanning astrometric instrument performs better if it spins faster, precesses faster, and has a shorter focal length than is conventionally expected. Further, we have shown that the use of solar radiation pressure instead of gas jets, as a means of precessing the spacecraft, yields a stronger astrometric solution, because the rotation is not broken into disjoint segments. Finally, we have shown that an elongated primary mirror is not advantageous, and that the central portion of the primary mirror contributes little to the astrometric accuracy of the instrument.

A first look at the pivotal issue of systematic error has uncovered no serious problems, although careful engineering will be essential. Because the spacecraft is equipped with a solar shield, which keeps it in shadow, the temperatures of critical instrument components are stable at the mK level on the time scale of the spacecraft rotation period. The analysis has underscored three instrumental differences between a survey astrometric mission and a pointed astrometric mission. For a survey mission, the aperture shape does not matter, a large-area detector enhances the scientific throughput, and there is no advantage to an interferometer over a telescope.

Keywords: Astrometry, space, instrument, optical

1. INTRODUCTION AND MISSION OBJECTIVES

Following the successful ESA mission Hipparcos,^{1,2} there has been interest in a follow-on astrometric survey mission that is even more capable. Several proposed missions have been studied, including ROEMER,³ DIVA,⁴ FAME,⁵ and GAIA.⁶ Here we report on the results of a 1½ year study of such an instrument to be known as the Fast Astrometric Mapping Explorer (hereafter, FAME-98^a), which has been a collaboration between the Smithsonian Astrophysical Observatory and the US Naval Observatory. The nominal requirement for FAME-98, established at the start of the study, is to measure at least 10^7 stars with an astrometric accuracy of 0.05 mas for mag < 9 and 20 mas for mag 15, and to perform color photometry with an uncertainty of under 0.25 mag for most targets. This paper describes a snapshot of an ongoing process intended to culminate

*Further author information

RDR: phone, 617-495-7108 (FAX '7109), reasenberg@cfa.harvard.edu

JDP: phone, 617-495-7360 (FAX '7109), jphillips@cfa.harvard.edu

^a FAME-98 should not be confused with the Fizeau Astrometric Mapping Explorer (FAME), which was the subject of an unsuccessful MIDEX proposal in 1995. For clarity, we will refer to it as FAME-95 hereafter.

in a MIDEX-class flight mission. At present, we have an initial instrument design in which many of the defining parameters have been set approximately, based on the studies described below. However, a global optimization has yet to be performed. FAME-98 takes from Hipparcos its two essential geometric characteristics, (a) the use of two widely separated look directions with the corresponding fields combined on a single detection plane, and (b) a scan pattern that involves both a nominal spin axis orthogonal to the look directions and the precession of that spin axis around the Sun direction. As the spin axis precesses, its angular separation from the Sun direction, ξ , remains approximately constant.

FAME-98 is a full-sky astrometric survey instrument with a calculated mission accuracy of better than $50 \mu\text{as}$ ($\mu\text{as}/\text{year}$) for bright stars ($m \leq m_0$, $11 < m_0 < 10$), based on the nominal mission length of 2.5 years. The astrometric parameters for most stars surveyed should be determined to an accuracy of better than 1 mas (mas/year). For a given star, the mission precision is derived from three factors: (a) the single measurement precision, (b) the number of measurements over the mission, and (c) the observing geometry. Optimizing the mission design includes trades between the first and second of these. The last of these may figure importantly, by way of parameter correlations and the condition number of the normal equations, when the astrometric parameters of the stars are estimated. However, we have not investigated this aspect of the design. The more subtle and highly significant issue of systematic error is briefly discussed at the end of the paper.

The instrument would support a mission that would survey the sky to determine the astrometric parameters of between 10^7 and 10^8 stars to a limiting magnitude at least as faint as 15. The five astrometric parameters of interest are position (2), proper motion (2), and parallax (1). In addition, the instrument would estimate the brightness (stellar magnitude) and temperature of the brighter stars. For a mag 9 star, the statistical uncertainties would be under 1 milli-magnitude and 10 K, respectively, but the systematic aspects of these uncertainties have not been addressed. The determination of brightness and temperature by the instrument will not be further addressed here, but are addressed briefly in the companion paper on the optical system.⁷ The FAME catalog is projected to be larger by 2 orders and more accurate by 1.5 orders than the Hipparcos catalog, which was a major advance in the art.

The principal objectives of the FAME-98 mission are to perform astrometric and photometric measurements of over 10^7 stars to determine their motion, parallax, and absolute brightness. The mission will support a rich and diverse ensemble of specific scientific investigations. Among the subjects to be addressed are: calibration of the standard candles (Cepheids and RR Lyrae), leading to a better cosmic distance scale; determination of parallax and thus absolute stellar magnitudes for a wide variety of stellar types, including both population I and population II stars; measurement of the space velocities of stars in the solar neighborhood; investigation of the dynamics of open clusters and OB associations; detection and characterization of companions, including stars, brown dwarfs, and planets; determination of the masses of stars in binary systems for a wide class of stars; improvement of the ephemerides of the outer planets and some of their brighter satellites; improvement of the ephemerides of the minor planets and the determination of the masses of some by means of mutual perturbations; and a light-deflection test of general relativity. From the star data will come: a better understanding of the internal structure of stars; the ages of clusters; an estimate of the density of dark matter in the Galaxy; and constraints on the mechanism responsible for the spiral arms. In addition, the mission will meet the needs of the USNO to provide a high-precision star catalog for the use of the DoD. For further discussion of the scientific applications of missions of this class, see ref. 5.

In Section 2, we describe the mission and present its nominal parameters, particularly in Tables A, B, and C. We also discuss the preliminary plan for the data reduction, which serves as a background for some of the studies and analyses discussed in Section 3. Some concluding comments are offered in Section 4, where we briefly address systematic error.

2. MISSION DESCRIPTION AND PRESENT NOMINAL

The FAME-98 mission has four principal elements: the instrument, mission operations, data analysis, and scientific interpretation. In the present instrument design, there is an Hipparcos-type field combiner (complex mirror), a three-mirror telescope with a square primary 0.56 m on a side, and a set of (nominally 22) CCD detectors. The two fields of view are separated by 64 deg, although our studies indicate that this separation is not critical. As the instrument rotates and the target images move across the surface of a detector array, the charge packet in the CCD is synchronously shifted. With this time-delay integration (TDI), the astrometric observable is the epoch at which the star centroid passes over the edge of the last row of the CCD.

The wide separation of the two fields of view makes FAME-98 a “global astrometric mission,” of which Hipparcos

has been the only flight example. Being a global astrometric mission yields three principal advantages: (a) the data contain 360° closure information, which results in a relative freedom from regional bias in the astrometric results; (b) the instrument measures absolute parallax, and there is no need to rely on so-called zero parallax objects (which is particularly important in directions of heavy obscuration); and (c) the analysis naturally yields a global reference frame, which supports comparison with other (e.g., radio) frames. Because it has a short focal length and uses many CCD chips in the detector plane, FAME-98 is able to measure many stars simultaneously. As compared to a pointed astrometric instrument of comparable size, FAME-98 (like other proposed survey instruments) has much higher scientific throughput (sum over targets of the inverse variance of position at the end of the mission), but on average, less scientific interest per target.

The parameters of the nominal FAME-98 instrument and spacecraft are shown in Tables A and B, respectively; a cartoon of the spacecraft is shown in Fig. 1. The large disc at the Sun-lit end of the cylindrical spacecraft is a solar shield that serves both to keep direct solar radiation from reaching the spacecraft and to provide the torque, by means of radiation pressure, to precess the spin axis as required for observing the full sky. Mission specifications are shown in Table C.

To understand the potential of any astrometric mission, one needs to consider the complete package that includes the instrument, the mission (i.e., data-taking particulars), and the analysis. All three will affect not only the nominal uncertainty in the positions of the observed stars, but also the systematic errors and the more subtle matter of the connection of the

measurements to a coordinate frame. *A fortiori*, it is essential to consider the complete package when attempting to optimize an astrometric mission. However, the process is iterative, and it is not yet possible for us to do a global optimization of the present instrument. Rather, some aspects of the mission have been established *pro tempore* and used as the framework for developing other aspects. In particular, we have used some of the spacecraft nominals from the FAME-95 mission (e.g., mass and moment of inertia), pending the resources to refine these quantities.

The intended data analysis method provides a context for some of the studies discussed in the next section. The Hipparcos Mission provided examples of data processing schemes that we used as the starting point for our present approach for FAME-98. The present (preliminary) FAME-98 data analysis approach has three stages starting from the determination of the event^b parameters:

(Stage A) The “observing-spiral” reduction (Hipparcos: great-circle reduction) would address the target events collected during a “batch interval” of from half a day to a few days and would yield a rotation model for the instrument during that period. In our studies, we assumed the analysis would use all stars from mag 8 to mag 10, about three per sq.

angle between spin axis and Sun direction (ξ)	45 deg
observation type	Time-Delayed Integration (TDI) -- yields “event times”
optical passband	0.4 to 0.9 μm , defined by the sensitivity of Si detectors
effective focal length	7.5 m
number of pixels across the diffraction pattern (n_s)	1.2
basic angle (between observing directions) (γ)	64 deg
focal plane	22 CCD arrays
CCD size	2k by 4k with 15 μm sq. pixels 0.4 arc sec / pixel
CCD noise level	5 e ⁻ or better
aperture (size of primary)	2 @ 0.5 × 0.25 m (0.56 × 0.56 m)
field of view	$\phi_{\text{outer}} = 2.2^\circ$ $L_{\text{inner}} = 1.1^\circ$ Area = 2.59 sq,deg.

^b In an astrometric system using TDI, the observable is the epoch of an event, which is the passage over the edge of the CCD detector of the centroid of the star image. This epoch is found by centroiding the image extracted from the CCD and using the resulting position estimate to interpolate the clock timing record.

size and shape of spacecraft	cylinder, 2 m by 2 m
mass	325 kg
moment of inertia	200 kg m ²
solar shield reflectivity of central circle (r = 1 m)	0.8 (assumes partial population by solar cells)
reflectivity of annulus (1 m < r < 3 m)	0.9 (assumes Al on plastic film)

nominal mission life	2.5 years
orbit	circular at about 100,000 km radius
rotation period	20 min ($\omega_z = 5.24 \cdot 10^{-3}$ /s)
precession period preferred method	10 days radiation pressure torque

deg, as the spiral-tie stars. The Stage-A analyses could be performed as soon as the target events are available from the first observing spiral. (Even a partial set could be used as part of the instrument check out.)

(Stage B) The global fit (Hipparcos: sphere solution) would interconnect the observing-spiral rotation models to yield a “global net” over the celestial sphere. It would be sufficient to have no more than 1000 global-tie stars, which would naturally be a subset of the spiral-tie stars, chosen for their even distribution over the sphere, their presence in the Hipparcos catalog, and their stable astrometric properties.^c The global fit could first be performed well (although probably for position only) after six to eight months of data-taking, about the time that full sky coverage is first available. After about a year, the analysis could be extended to include proper motion and parallax.

(Stage C) The application of the models and parameters determined during the first two stages (Hipparcos: astrometric parameter determination) to the determination of the astrometric parameters of the program stars would create the catalog.

Note that during Stages A and B, the objective is to develop a rotation model for the instrument, not to estimate the astrometric parameters of the target stars. It is only in Stage C that stellar astrometric parameters are estimated and preserved.^d At all stages, the analysis must include the identification and modeling of non-point targets. (This modeling is not addressed here.) Most of the global-tie stars would be mag 9 or brighter. By virtue of the selection process, they would be well measured by Hipparcos; there would be reasonably good *a priori* values for their astrometric parameters, except in some interesting cases of peculiar motion not identified during the short Hipparcos mission.

To iteratively clean up the solution, the Stage-C procedure would be applied to the combined set of spiral- and global-tie stars only. With improved estimates of positions, proper motions, and parallaxes for these tie stars, the observing-spiral reductions and global fit would be repeated. Unless this iteration uncovers and precipitates the removal of bad data (blunders) or shows some of the tie stars to be unsuitable, it is unlikely that it would *need* to be repeated, although the convergence rate remains to be investigated. However, to improve the catalog that forms the basis for various near-real-time analyses, we would likely perform such an iteration a

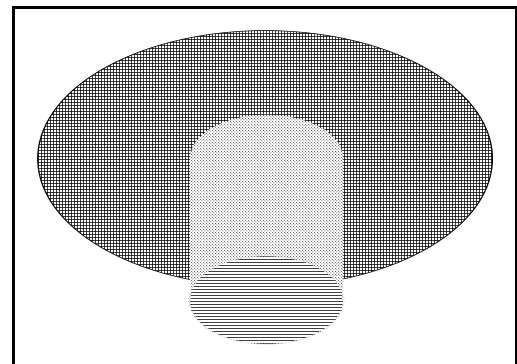


Figure 1. Cartoon of spacecraft showing the solar shield (disc) and body (cylinder). The view of the shield is of the unilluminated side.

^c There would be no harm in changing global-tie stars after the analysis had started.

^d During Stages A and B, stellar astrometric parameters could be estimated but not saved. However, according to the present (preliminary) plans, a numerical technique for speeding up the analysis will bypass the estimates of the star positions.

number of times, beginning as early as possible in the mission. The first such iteration could be after about six (or eight) months of data taking, when we first have full sky coverage. These additional analyses would serve to detect problems early in the mission.

For many purposes, the orientation of the reference frame is not important. However, intercomparisons of the FAME-98 star catalog with other data would be facilitated by providing a standard orientation, which is connected to the Earth ecliptic and equator. The ecliptic has only a little meaning in a spaceborne astrometric study, where it enters through aberration, and the equator has none. However, a reasonable frame orientation can be assured by using standard catalog positions for the *a priori* position estimates for the spiral- and global-tie stars. Even if these were given modest uncertainties, say 10 mas, they would anchor the frame well.

3. SEVEN KEY RESULTS OF THE STUDY

The present instrument design is based on seven results from recent studies plus the conclusions that have followed from the optical analyses described by Phillips and Reasenberg (in these proceedings, Ref. 7). It is supported by a preliminary thermal analysis, which is summarized in Section 3.5. The seven results are listed below and discussed in the following sections.

- a) Central obscuration of telescope does not matter (much).
- b) The aspect ratio of the primary mirror (or pupil) does not affect “information rate.”
- c) Smooth rotation of the instrument is highly desirable; mission accuracy is impaired if attitude correction events are as frequent as one per rotation. (Hipparcos corrections occurred about 12 times per rotation.)
- d) Solar radiation pressure (instead of gas) can be used to precess the spacecraft.
- e) The basic angle (γ) is not critical, as long as a few bad angles are avoided and γ is chosen not far from 90 deg.
- f) For a focal plane of fixed size, and over accessible values of the effective focal length, \mathbb{F} , the “information rate” varies slowly with \mathbb{F} , and favors small \mathbb{F} .
- g) The Hipparcos-type scanning pattern gives good sky coverage, independent of ξ .

3.1 Central obscuration

Lindgren⁸ has investigated the astrometric accuracy of an instrument with an aperture of arbitrary shape. He showed that in the case of noise due to photon counting statistics

$$\sigma = \frac{\lambda}{2\pi L_{\text{rms}} \sqrt{N}} \quad (1)$$

where N is the number of detected photons and L_{rms} is the effective aperture width. Consider a rectangular aperture of length S (in the sensitive or scan direction) and width C (in the cross-scan direction) with a central obscuration of length κS and full width. It is easily shown by direct evaluation of the Fraunhofer integral that the information rate is

$$B = \sigma^{-2} \propto S^3 C (1 - \kappa^3) / \lambda^2 \quad (2)$$

For a generous central obscuration, $\kappa = 0.4$, there is only a 6.4% loss of information. However, it is apparent that there is an incentive to make an astrometric instrument as big as possible in order to maximize its accuracy. For faint stars, Eq. 1 must be generalized to include detector noise. It remains to be shown that Eq. 2 applies in the faint-star case.

3.2 Mirror aspect ratio

Equation 2 tells us that, for an astrometric instrument, it is advantageous to deploy the mirror area over an extended distance

in the direction of the intended astrometric measurement. Further, for fixed area, it is advantageous to separate the primary into two parts at considerable distance, again along the intended direction of measurement. These conclusions are correct for a pointed instrument. However, for a survey instrument, the total information rate, I , is proportional also to the region of sky, $\Omega = PQ$, that can be seen at a given time, where P and Q are the field of view in the scan and cross-scan directions, respectively. For a single CCD chip, P and Q depend on the number of pixels (N_s and N_c), the pixel size, w , and the focal length.

We start the analysis with the case of unlimited anamorphism: the focal lengths, f_s and f_c , are independent quantities.

$$P = \frac{N_s w}{f_s} \quad Q = \frac{N_c w}{f_c} \quad (3)$$

For a representative wavelength ($\lambda = 0.6 \mu\text{m}$), let n_s (n_c) be the number of pixels across the full width at first null of the diffraction pattern of the primary, excluding the effect of the central obscuration. Then, $2\lambda/S = n_s w/f_s$, $2\lambda/C = n_c w/f_c$, and using the above, we find

$$P = \frac{2N_s \lambda}{n_s S} \quad Q = \frac{2N_c \lambda}{n_c C} \quad (4)$$

Combining Eqs. 2 and 4, we obtain

$$I_u \propto BPQ \propto S^2 \frac{N_s N_c}{n_s n_c} \quad (5)$$

This is a surprising result: With unlimited anamorphism, the information rate is independent of the width of the mirror. This result arose because we required that the number of pixels across the image be fixed, presumably at a small value. This would be required in the actual mission so as to preserve some cross-scan information for determining the spacecraft orientation.

We next consider the more realizable case of fixed anamorphism, $f_s = \alpha f_c$, where we will later require $\alpha = 1$. Eqs. 3 take the form

$$P = \frac{N_s w}{f_s} \quad Q = \frac{N_c \alpha w}{f_s} \quad (6)$$

and only the left of Eqs. 4 will apply. Again, combining expressions, we obtain

$$I_\alpha \propto BPQ \propto SC \alpha \frac{N_s N_c}{n_s^2} \quad (7)$$

which is also a surprising result: The information rate depends on the mirror area and is independent of its shape. We are thus free to select a mirror aspect ratio that is convenient to manufacture and mount, and that will be mechanically (and thermally) stable. For a rectangular mirror, the obvious choice is approximately square. This conclusion should apply to GAIA as well as FAME-98.

3.3 Smooth rotation and the basic angle

Hipparcos scanned the sky by means of a series of attitude correction events (ACE) using gas jets. These events occurred on average at intervals of about 12 minutes. We have investigated the first stage of ground-based data reduction for FAME-98, the observing-spiral reduction, corresponding to the great-circle reduction in the Hipparcos analysis. For this purpose, we simulated mission data using the same set of Monte Carlo stars for all cases. These stars had a mean density of 3 per square deg, consistent with using all stars from mag 8 to mag 10. Over a batch interval, we introduced a series of ACE. The spans between successive ACE were drawn from a Gaussian distribution, typically with a variance equal to 0.25 of the mean. The simulated data were analyzed by the weighted-least-squares (WLS) method in which we assigned uncertainties of 0.35 and 3.5 mas to the measurement components in the scan and cross-scan directions, respectively, and assumed an *a priori* knowledge of the star coordinates with uncertainty of 10 mas in each direction. The data were fit to a model including two position parameters for each star, some instrument parameters, including γ , and a set of spacecraft rotation model parameters. For each of the spans, the rotation model included the precession phase and rate, ξ and its rate, and a series for the rotation phase,

$$\varphi = \varphi_0 + \sum_n A_n P_n(t) \quad (8)$$

where $P_n(t)$ are Legendre polynomials and the time, t , is normalized to be zero at the center of the span and ± 1 at the ends.

Of primary concern in these studies was the degree to which the observing spiral was tied together by the observations. To investigate this, we introduced a series of pseudo-observations of the rotation phase $\tilde{\varphi}$, and used standard error propagation to determine $\sigma(\Delta_j)$, where Δ_j is a spacecraft rotation by an angle proportional to j .

$$\begin{aligned} \sigma(\Delta_j) &= \text{AVG}_{(n=1, \max)} [\sigma(\tilde{\varphi}_{n+j} - \tilde{\varphi}_n)] \\ \text{Log}_{10} \bar{\sigma} &= \text{AVG}_{(j=\text{range})} [\text{Log}_{10} \sigma(\Delta_j)] \end{aligned} \quad (9)$$

where in the second equation, the range of j is chosen such that the average is approximately over the first 2.5 spacecraft rotations following the first half rotation. (One can well imagine other useful measures.) In general, plots of $\sigma(\Delta_j)$ vs Δ_j show a lobate structure with dips at multiples of the rotation period. Plots of $\text{Log}_{10} \bar{\sigma}$ vs γ show a broad minimum centered at about $\gamma = 100$ deg, with spikes at “bad angles” such as 180, 120, and 90 deg. Within the range from 70 to 130 deg, $\bar{\sigma} < 1.1$ times the best $\bar{\sigma}$, except at the spikes. When the mean length of the spans between successive ACE was increased from 1/6 of the rotation period to the rotation period, we found that $\bar{\sigma}$ was lowered by a factor of 4.4. When the span length was made equal to the batch length of the observing spiral (6 rotation periods), $\bar{\sigma}$ was lowered by a factor of 11 from the original value. We conclude that it is highly desirable to avoid ACE, and that decreasing their frequency is of great importance. (Details of this study will be published elsewhere: Chandler and Reasenber, in preparation.)

Based on the broad minimum centered at about $\gamma = 100$ deg in plots of $\text{Log}_{10} \bar{\sigma}$ vs γ , we were free to consider other factors in selecting γ . In order for the light from the target stars to clear the primary mirror on the way to the complex mirror, γ must be greater than 58 deg. When baffling is added, this increases to $\gamma \geq 64$ deg. The construction of the complex mirror is simplified, and its structure is made most stable, by keeping γ small. We have therefore tentatively selected 64 deg for the basic angle.

3.4 Precession by means of solar radiation pressure

Figure 1 is a cartoon of the FAME-98 spacecraft showing a large flat solar shield, perpendicular to the nominal spin axis. Light specularly reflected by this shield produces a force parallel to the spin axis and through the center of figure, which we assume lines up with the center of mass. Light that is absorbed produces an additional force in the plane of the shield and thus a torque that tends to increase ξ , the angle between the spin axis and the Sun direction. For a spinning spacecraft, this torque causes a precession around the Sun direction.

Tables B and C contain the nominal spacecraft and mission specifications. Based on these, we find: angular momentum, $J = I\omega_z = 1.05 \text{ kg m}^2 / \text{s}$; torque from radiation pressure, $N = 7.13 \cdot 10^{-6} \text{ Nm}$; and precession rate due to the torque, $\Omega = N / J = 0.47 \text{ deg per spacecraft rotation}$. This is at about the limit, $\Omega_{\text{max}} \approx 0.5 \text{ deg per spacecraft rotation}$, set by the requirement that a star image spread across only a few columns of the CCD detector chip as that image traverses the chip in the scan direction. Too great a deviation from the desired image path would result in an unacceptable loss of cross-scan information.

A small adjustment to the shape of the solar shield causes a significant change in the solar torque. In particular, for the nominal parameters, $(1/N) dN/d\alpha = -0.6 \text{ per deg of shield tilt}$. (See Fig. 2 for a definition of α .) There are myriad reasons to want to change the torque. Fortunately, the sensitivity of N to α provides for a large range of adjustment of N without making the shield excessively non-flat (in the sense discussed in the next section).

As discussed in the previous section, the use of radiation pressure to precess the spacecraft significantly increases the mission accuracy by eliminating most of the gas-jet firings needed for attitude correction. Further, since the gas will not be essential after the initial set-up of the spacecraft, the risk presented by relying on the gas-jet thrusters will be eliminated. This enhanced reliability can help extend the mission beyond the nominal life, although the return on that extension has not yet been investigated.

3.5 Thermal considerations

Our design philosophy for FAME-98 has been to achieve high astrometric accuracy with a minimum of complexity. In keeping with this philosophy, we use thermal control but not laser gauges to maintain the configuration of the instrument. The prime requirement of the thermal control is stability. We are particularly concerned with temperature variation at the spacecraft rotation frequency and its harmonics, since these would map into repeatable measurement biases related to sky position. The first stage of the thermal control is provided by the round Sun-facing solar shield, which is shown in Fig. 1. The shield prevents sunlight from directly reaching the surface of the spacecraft.

In the absence of the shield, the spacecraft would experience “rotisserie heating” and there would likely be a corresponding instrument bias varying at the rotation frequency. *If the shield is flat*, and ignoring heat from the spacecraft and Earth, the shield will be isothermal, and there will be *no* rotisserie effect. The spacecraft will preferentially heat the shield near it, causing a temperature distribution on the shield that rotates with the spacecraft, which is benign. Below, we look at the thermal input along the cylindrical spacecraft wall, at the effect of a non-flat shield, and at the thermal input from Earth, which sets the scale for useful solar shielding.

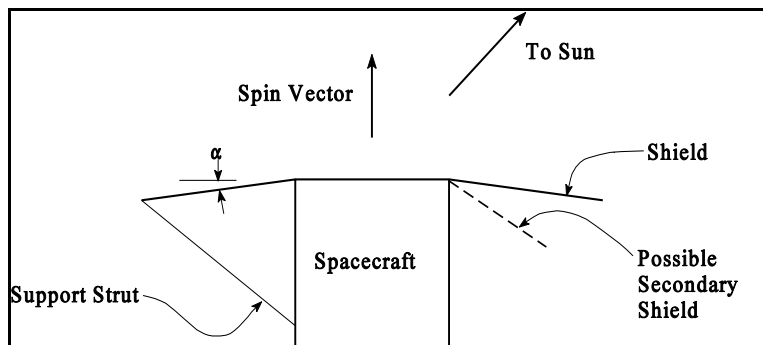


Figure 2. Spacecraft with secondary shield, which is now not believed to be necessary.

In the calculation of thermal radiative transfer, the analysis is normally broken into two stages: geometric and thermal. The first stage yields the “coupling factors” between the elements of the problem, the radiating surfaces. The second stage is the iterative solution of a set of non-linear heat equations. The Geometric Configuration Factor (GCF, see Siegel and Howell,⁹ especially chapter 6) is the quantity calculated during the first stage. F_{1-2} is a GCF defined as the fraction of the energy leaving surface #1 that arrives at surface #2. It can be shown that F_{1-2} is also the fraction of the weighted

solid angle through which surface #1 receives energy from surface #2, where the weighting factor is $\cos(\theta)$ and θ is the angle between the normal to surface #1 and the look direction to surface #2. For a point on the spacecraft wall next to the shield, it is easy to show that the shield has $F = 1/2$. The following factors yield the input to the spacecraft wall next to the shield: (1) solar flux, $S = 1360 \text{ W/m}^2$; (2) $\cos(\xi) = 0.7$; (3) $(1 - R_2) = 0.1$, where R_2 is the reflectivity of the shield, which we take as 0.9; (4) 0.5, because the shield radiates equally from both sides (the shield is assumed isothermal -- non-insulating -- and the emissivity is assumed equal on both sides of shield); and (5) $F = 1/2$, because the shield fills half of the (weighted) solid angle. When combined, these yield 24 W/m^2 . A calculation of the GCF shows that at a point on the spacecraft wall about 1.4 m from the shield, where the instrument is expected to be, F is lower by a factor of 3, yielding a heat input of 8 W/m^2 .

If the cylindrical wall surface were black and at 300 K, it would radiate 460 W/m^2 . To radiate an additional 8 W/m^2 , the temperature must increase by 1.3 K. Without the shield, the flux would be $S \sin(\xi) \Phi$, where $\Phi = \{\cos(\nu), 0\}$: depending on whether the patch is sunlight or in shadow and ν is the Sun's azimuth with respect to the point of interest on the wall. The average flux would be smaller by π than the peak value of $S \sin(\xi)$. Thus, in the vicinity of the instrument, the shield provides a 40 fold reduction from the average flux and, far more importantly, it provides a constant flux.

The shield may need to be tilted away from the Sun by a small angle (a few degrees). The sweep back will change the shield temperature. The primary effect is the change in the angle ζ between the shield normal and the direction to the Sun. This results in a shield temperature that depends on ν , the rotation phase. In particular, the power input to the shield is proportional to $\cos(\zeta)$:

$$\cos(\zeta) = \cos(\alpha) \cos(\xi) + \sin(\alpha) \sin(\xi) \cos(\nu) \quad (10)$$

Of the two terms on the right hand side, the first yields an uninterestingly small shift in temperature for reasonable values of α (say $|\alpha| < 10 \text{ deg}$). The second results in a time variation of the shield temperature with spacecraft rotation. For $\alpha = 2 \text{ deg}$, the 8 W/m^2 received from the shield at the instrument has a periodic component of about 0.25 W/m^2 amplitude that could cause a corresponding temperature variation of 0.04 deg.

In considering the heat input from the Earth, we make the simplifying assumption that it is a black body at 300 K, and we initially ignore both the extra heat that comes from reflected sunlight on the day side, and the difference between the thermal IR and reflected light received by the spacecraft when it is over the pole and when it is over the equator. For a spacecraft at $16 R_e$ from the Earth ($15 R_e$ above the surface, where R_e is the radius of Earth), the GCF is easily shown to be $F = 0.004$ for a surface facing Earth. The corresponding heat absorbed by a black surface is 1.84 W/m^2 . Note that the input on this surface will vary at the spacecraft rotation rate and be modulated by the spacecraft orientation with respect to the nadir. In the worst case, when the spacecraft spin axis is perpendicular to the Earth direction, the rms variation is 0.27 W/m^2 . To radiate an extra 1.84 W/m^2 , a black surface at 300 K must warm by 0.3 K. The factors ignored above increase the complexity of the temporal signature of the thermal input. Note that the phase-dependent heat input from Earth is several times the phase-dependent heat input from the Sun, even if α is large. Thus, further reduction by the shield of the solar heating would not be helpful.

3.6 Telescope effective focal length

In Section 3.2, we found that the optimal shape of the aperture is not long and thin when one includes the effect of sky coverage in the calculation of the total information return. Here we apply the same concept to the question of the plate scale, i.e., the number of pixels to cover the diffraction pattern. In particular, for the nominal wavelength ($\lambda = 0.6 \mu\text{m}$), n_s (n_c) is defined as the number of pixels across the full width at first null of the diffraction pattern of the primary, excluding the effect of the central obscuration. It is easily shown that, neglecting detector noise, the single-object information rate \mathfrak{R}_1 is monotonic with n_s . But, for a survey instrument, the quantity of interest is \mathfrak{R}_d , the rate of information collection by the entire detector. As we found in Eq. 5, there is an extra factor of $1/n_s n_c$. In the absence of anamorphism

$$\mathfrak{R}_d \propto \mathfrak{R}_1 / n_s^2 \quad (11)$$

This is the quantity that is shown in Fig. **Figure 3** for the two cases discussed below.

To calculate \mathfrak{R}_d , we simulated the photon counts in the pixels covering several fringes near the center of the diffraction pattern. We then performed a WLS fit to one of two models. In the first, there was only one free parameter, p , the position of the star in the scan direction. In the second, there were two additional free parameters, the brightness of the star, and its temperature, assuming it to be a black body. In both cases, for small values of n_s , $\sigma(p)$ was found to depend on the phase of the star, i.e., its position with respect to the pixel boundary. Each quantity shown in Fig. **Figure 3** reflects an average of information over that phase.

Inspection of Fig. **Figure 3** shows that, over a large range of n_s , the total information rate increases as n_s gets smaller. This is so even though the information from a single measurement of a star increases with n_s . Fig. **Figure 3** suggests that we should use $n_s = 0.6$. However, the present optical system does not work well at the required short focal length of 3.75 m. In the companion paper (see ref. 7) on the optical system, we discuss the options. For now, we use a focal length of 7.5 m and $n_s = 1.2$. Further, as $n_s \rightarrow 0$, the information about a particular star comes increasingly from a small subset of the observations of that star which fall on the pixel boundary. Although the number of strong observations increases with decreasing n_s , for small n_s , the increase is slowed.

3.7 Scanning pattern

It is intended that FAME-98 will use a version of the Hipparcos observing pattern in which the spacecraft spins to allow the observation of stars in two directions fixed in the (rotating) plane perpendicular to the nominal spacecraft spin axis, and the spin axis slowly precesses around the Sun direction. The angle between the spacecraft spin axis and the Sun direction, ξ , is bounded at the high end by the Sun avoidance requirement and at the low end by the need to observe each star from a variety of angles, which reduces estimator degeneracy. The first objective of the scanning-pattern study was to address the value of ξ . Are there values of ξ that are especially good (or bad)? Is it important that ξ be held constant, or that it is allowed to change over the mission? The second objective was to determine as a function of the ecliptic latitude (b) the (local) azimuthal uniformity of the star-position information, which bears on the shape (aspect ratio) of the error ellipse of measured star positions (i.e., the relative uncertainties in estimates of b and $\ell \cos(b)$, where ℓ is the ecliptic longitude).

In principle, a complete and definitive answer to these questions would come from full mission simulations, including a covariance analysis of the simulated data. This has not been possible. Instead, we have taken a first look by investigating the density of observations in b , based on a single spacecraft look direction. The independent variable is taken as $\cos(b)$ because, for a uniform distribution over the sphere, the density in $\cos(b)$ is flat. No consideration is given to the density in ℓ , and the results may be considered an average over ℓ . To address the second objective, we examined the range and distribution of observing directions of stars as a function of b .

The required density of observations can be obtained analytically in terms of the Incomplete Elliptic Integral of the First Kind. Instead, we used a direct numerical approach, which has the advantage of being able to accommodate additional

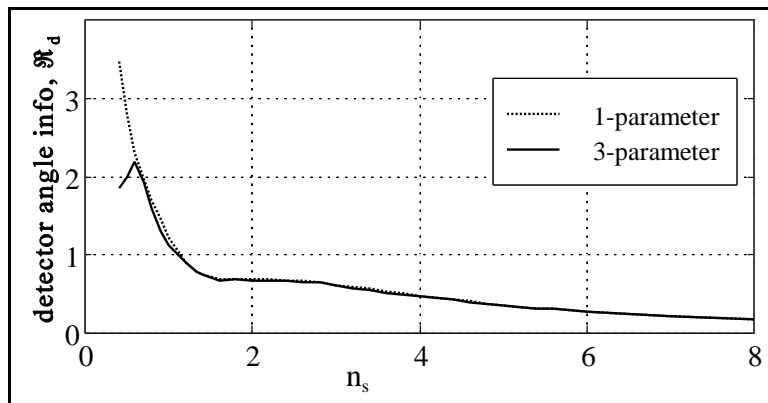


Figure 3. Full-detector information rate \mathfrak{R}_d (arbitrary units) vs n_s , which is proportional to effective focal length. Calculation was at $m_{bol} = 9$, with no read noise. Note that \mathfrak{R}_d was calculated at intervals of 0.2; finer steps might round the turnover at $n_s = 0.6$.

complexities as they arise. There are two independent variables over which integrations are required: the precession angle of the spacecraft spin axis around the Sun direction, and the rotation phase of the spacecraft. Two approaches were taken to the numerical integration, direct and Monte Carlo. The results were essentially the same, and the former was used for the analysis shown here. Figure 4 shows the observation density for three values of ξ : 35, 45, and 55 deg. The curves are normalized to an average of 1, and the fine irregularities are artifacts of the integration method. It is easily shown that the peaks seen in each case are at $90^\circ - \xi$. For the case of $\xi = 45^\circ$, the lowest point is at $b = 0$, and has a density of 0.75. Thus, although the distribution is far from flat, there is little loss of accuracy of star position estimates. Further,

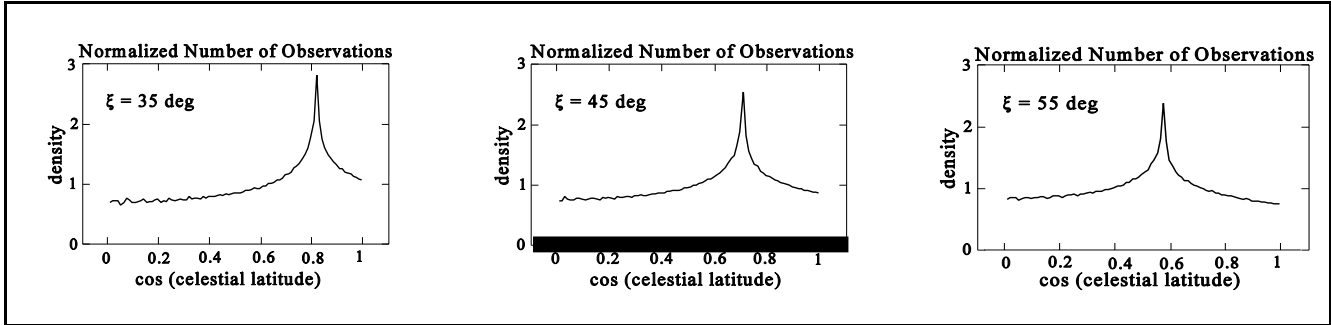


Figure 4. Density of observations for three values of ξ , the angle between the Sun direction and the rotation axis.

the exact value and stability of ξ do not seem to matter.

The second objective was addressed by using the same software to produce a two-D histogram of observation density as a function of $\cos(b)$ and the angle between the local meridian and the spacecraft observation direction. The histogram shows a non-uniform distribution (different for all three values of ξ), but the non-uniformity is unlikely to produce a substantial elongation of the error ellipses.

4. DISCUSSION

We have investigated several aspects of a MIDEX-class astrometric survey mission. For many non-critical aspects of the mission, we have used the nominals from the FAME-95 mission proposal. For critical aspects of the instrument, we have developed a new set of nominal designs and parameter values. Some important questions remain open. Among these is the telecommunication system design and downlink rate. The present instrument design yields a massive set of data. Considerable reduction in the download requirement (3 to 10 fold) may be possible by means of on-board processing (e.g., centroiding) of the CCD output. But this approach is not without a potential loss of astrometric information.

While the nominal parameters of the mission have not been globally optimized, we believe that they are close to correct. It is therefore worth making a comparison with the corresponding aspects of FAME-95. As shown in Table D, compared to FAME-95, FAME-98 has a more compact aperture, larger field of view, shorter focal length, faster spin and precession, and longer uninterrupted observing spans between attitude control events. Further derived mission characteristics are shown in Table E.

The analysis has underscored three differences between a survey astrometric mission and a pointed astrometric mission. For a survey mission, the aperture shape does not matter; for a pointed mission, it is better to have an elongated aperture. For a survey mission, a large-area detector enhances the scientific throughput because it catches more targets per unit time; for a pointed mission, once there are enough detector cells to work with a single target, additional detector cells will not, in general, help except to facilitate acquisition. For a survey mission, we find no advantage to an interferometer over a telescope; for a pointed mission, it is well known that an interferometer offers considerable advantage (for fixed aperture area). We speculate that this observation can be generalized to a theorem. For spaceborne astrometric instruments, a telescope is appropriate for a survey mission, and an interferometer is appropriate for a selected-target (i.e., pointed) mission.

A central theme of astrometry is concern for systematic error. For FAME-98, we have identified three principal potential sources of instrumental systematic error: thermally induced changes in the instrument geometry, response of the optical system (including the detector), and spacecraft rotation. In addition, systematic error can come from improper modeling of target structure, which is not addressed here. In each case, once the potential source of error is identified, a mitigating approach can be developed.

Table D. Mission Comparison		
Aspect	FAME-98	FAME-95
Shape of Aperture	Square	Elongated
Number of reflections	5 (inc. 2 flats)	8 (inc. 2 flats)
Field of View* (Area in sq. deg.)	$\phi_{\text{outer}} = 2.2^\circ$ $L_{\text{inner}} = 1.1^\circ$ Area = 2.59	$\phi \approx 0.66^\circ$ Usable part $\approx 0.26^\circ$ wide Area ≈ 0.122
Effective Focal Length	7.5 m	36 m
Spin Period	20 minutes	2+ hours
Precession Period	10 days	60 days
Precession Method	Solar Radiation Pressure	Cold Gas Jets
Mean Time Between Attitude Correction Events	days	≈ 20 minutes

* The field of view of FAME-95 is a D-shaped region between the circumference of the circle (of 0.66° diameter) and a chord about 0.26° from the center of that circle.

significantly to the error budget (of a mag 9 star). Crude arguments lead to a similar preliminary conclusion for the other optical elements of the system.

The response of the optical system includes telescope distortion, which is addressed in the companion paper, ref. 7. At the detector, the depth of penetration depends on color, and ranges from less than $1\mu\text{m}$ for $\lambda = 0.4\mu\text{m}$ to tens of μm for $\lambda = 0.9\mu\text{m}$. For the f/13 beam at the detector, this results in a "chromatic blur." Further, since the system is not telecentric, there is a lateral displacement associated with the depth of photon penetration, and thus a color dependence of the apparent position of the target. This chromatic effect can be corrected in the data analysis, given even a coarse spectrum of the target.

To lowest order, the spacecraft can be expected to rotate smoothly. However, at the sub-milliarcsecond level, there will be significant deviations from smooth rotation. One traditional source of rotation irregularity, thruster leaking, should not be a problem with the attitude-control gas jets not in use. Outgassing of volatiles should decay during the early months of the mission. However, this needs to be addressed quantitatively. Radiation pressure will interact with deviations from spacecraft axial symmetry to produce torque around the spin axis. For example, a patch of darker material on the Sun shield will cause the spin rate to vary sinusoidally with rotation phase. If a square meter of the shield at 2 m from the center has a reflection coefficient of 0.89 instead of 0.90, there will be a periodic rotation error of about 2 arcsecond. Of course, this will be a stable

or slowly changing feature that can be modeled well. Similarly, the radiation from Earth entering the view ports will hit dark surfaces and produce rotational variations of arcsecond order. Based on our covariance studies, we believe that if these and similar effects can be modeled phenomenologically, the corresponding parameters can be estimated with little impact on the precision of the astrometric parameters.

Table E. Mission Characteristics.	
number of target stars	about $4 \cdot 10^7$
average number of measurements per star	6000
transition magnitude (variance increased two fold by read noise)	$\sqrt{15.3}$

^e It follows that other elements will receive some of the reflected radiation. Consideration should be given to a shutter to protect both the detector and the optical elements.

A further complication to the smooth rotation of the spacecraft is the solar wind. Although it contributes only about 0.1% as much pressure as sunlight, it is highly stochastic. Further, the spacecraft surfaces will be non-reflective to the wind, and its apparent direction is shifted by virtue of the motion of the spacecraft with respect to the Sun. Some aspects of this problem are being investigated by M.A. Murison (USNO, private communication, 1997, 1998).

The optical system has provision to extract the central portion of the field of view, about 1.1 deg square. This could be relayed to a second instrument, which could have, for example, a long focal length, a dispersive element, and a separate set of CCD detector chips. A second instrument of this kind would provide more detailed spectral information and some finer spatial resolution for a large subset of the brighter targets. The cutoff for this instrument would be a few (say 4) mag higher than for the main instrument because of the longer focal length and the dispersion, both of which spread the light onto a larger number of pixels. (With a long focal length, it would not be economically possible to fully populate the focal plane with detector chips, nor would it be necessary in order to observe most of the brighter targets a few times during the mission.) The additional information from the second instrument could support target modeling and the reduction of biases associated with source structure, which are particularly important for the brighter targets. That information could also support the scientific interpretation of the estimates of star temperatures, as discussed in Section 3.6. Should this calibration prove successful, there would be a new method of estimating star temperature, and it would require neither filters nor a dispersive element

5. ACKNOWLEDGMENTS

We thank M.A. Murison and P.K. Seidelmann for a careful review of the draft manuscript, and J.F. Chandler for allowing us to present his work on spacecraft rotation and the basic angle prior to publication. The work described here has been supported by the U.S. Naval Observatory and the Smithsonian Institution.

6. REFERENCES

1. The Hipparcos and Tycho Catalogues, ESA SP-1200, 1997.
2. M.A.C. Perryman *et al.*, The Hipparcos Mission, ESA SP-1111, Paris, 1989.
3. U. Bastian, G. Gilmore, J.L. Halbwachs, E. Høg, J. Knude, J. Kovalevsky, A. Labeyrie, F. van Leeuwen, L. Lindegren, P.W. Pel, H. Schrijver, R. Stabell, and P. Thejll "ROEMER, Proposal for the Third Medium Size ESA Mission (M3)," Lund, 1993 (available from L Lindegren on request).
4. S. Röser, U. Bastian, K.S. de Boer, E. Høg, H.P. Röser, C. Schalinski, E. Schilbach, C. de Veigt, S. Wagner, "DIVA – Towards Microarcsecond Global Astrometry," Proceedings of the Hipparcos Venice '97 Symposium, Venice, May (13-16) 1997, <http://astro.estec.esa.nl/Hipparcos/venice.html#session12>.
5. K.J. Johnston, P.K. Seidelmann, *et al.*, "Fizeau Astrometric Mapping Explorer (FAME)," in preparation., 1998.
6. L. Lindegren, M.A.C. Perryman, and S. Loiseau, "Global Astrometric Interferometer for Astrophysics (GAIA)," SPIE Proceedings 2477, 91-103, 1995.
7. J.D. Phillips and R.D. Reasenberg, "Optical system for an astrometric survey from space," paper 3356-114 in these proceedings, 1998.
8. L. Lindegren in *Modern Astrometry*, F.V. Prochazka and H.R. Tucker, eds., IAU Coll. 48, 197-217, 1978; See also Lindegren *et al.*, SPIE 2477, *op cit*.
9. R. Siegel and J.R. Howell, *Thermal Radiation Heat Transfer*, Hemisphere Publishing, Washington, 1992.